CELL DISAGGREGATION BEHAVIOR IN SHEAR FLOW

PATRICK SNABRE, MICHEL BITBOL, AND PIERRE MILLS
Laboratoire de Biorhéologie et d'Hydrodynamique Physicochimique, Université Paris VII, 75251 Paris Cedex 05, Paris, France

ABSTRACT The disaggregation behavior of erythrocytes in dextran saline solution was investigated by a light reflectometry technique in a Couette flow and in a plane Poiseuille flow. Dextran concentration and mass average molecular weight of the polymer fraction strongly influence the shear stress dependence of the erythrocyte suspension reflectivity in shear flow and the critical hydrodynamic conditions (shear rate or shear stress) for near-complete cell dispersion. We investigated the influence of cell volume fraction and membrane deformability (heat treatment of the erythrocytes) on the reflectivity of the flowing suspension. This study indicates that the intercell adhesiveness and the shear stress are the only parameters that influence rouleau break-up in steady uniform shear flow, thus eliminating cell volume fraction and membrane deformability as possible factors. However, the critical cross-sectional average shear stress for near-complete cell dispersion through the flow cross-section is shown to depend on the flow pattern. The rotation of cells in a shear flow or the nonuniform shear field in Poiseuille flow indeed increases the flow resistance of cell aggregates. We give a theoretical description of the shear-induced cell disaggregation process in Couette flow and in plane Poiseuille flow. The quantitation of shear forces for cell dispersion provides a way for estimating the surface adhesive energy of the bridging membranes by fluid mechanical technique.

INTRODUCTION

Red cell aggregation plays a prominent role in the shear-thinning behavior of blood in low flow states (1). It has long been known that fibrinogen and some globulin fractions present in the normal blood plasma are involved in cell adhesion and rouleau formation (2, 3). The phenomenon of reversible erythrocyte aggregation has been already extensively studied from the standpoint of the interaction forces at cell surfaces (4, 5). The adhesion of red blood cells (RBCs) by the neutral polymer dextran represents an ideal system for elucidating the fundamental mechanisms of cell-to-cell interactions. During the last ten years, more and more evidence has been provided that erythrocyte aggregation results from the macromolecular bridging between adjacent cell surfaces (6–8). In the absence of mechanical shearing, steric repulsion forces arising from the loss of configurational entropy of bridging macromolecules and repulsive electrostatic forces due to the presence of negative charges on the outer membranes balance the surface adsorption forces (9, 10, 19). The work done by fluid mechanical forces helps to overcome the net adhesive energy between cell surfaces, and sufficiently high fluid stresses lead to erythrocyte disaggregation. The quantitation by fluid mechanical technique of the intercell adhesive energy still remains one of the major problems in hemorheology, which requires a study of rouleau break-up phenomena in steady flow.

We first investigated by a laser light reflectometry technique the effect of cell volume fraction and membrane properties on rouleau break-up in Couette flow. The identification of intercell adhesiveness and shear stress as the only parameters that influence rouleau break-up in uniform-shear flow then led us to compare the erythrocyte disaggregation phenomena in different hydrodynamic situations (e.g., Couette flow, plane Poiseuille flow, flow channel technique introduced by Chien's group [11] and consisting in the observation of the degree of cell separation of an isolated doublet attached to a channel wall and being subjected to a shear force parallel to the bridging interface). Moreover, we consider in a theoretical section the influence of a plasma layer on cell disaggregation behavior in Couette flow and plane Poiseuille flow. The present study of the factors affecting rouleau break-up in steady flow is of fundamental interest for determining cell adhesive energy by fluid mechanical technique and for estimating the importance of RBC aggregation in the microcirculation.

MATERIALS AND METHODS

Materials

Blood was obtained from healthy human donors anticoagulated on CPD and used on the day of withdrawal. After centrifugation and removal of plasma and buffy coat, the RBCs were washed twice in isotonic phosphate-buffered saline solution (PBS) (151 mM NaCl, 5.6 mM KCl, 5.5 mM Na_2HPO_4, and 0.3 mM NaH_2PO_4; pH 7.4 and O = 300 mosM/kg). The polymers dextran T40 (DX 40), T 80 (DX 80), T 500 (DX 500) (Pharmacia Fine Chemicals, Uppsala, Sweden), and dextran T 150 (DX 150) (Sigma Chemical Co., St. Louis, MO) were dissolved in PBS at concentrations up to 8 g% (wt/vol). Absolute average molecular weights (MWs) of dextran fractions were determined by combination of

Dr. Bitbol's new address is Institut de Biologie Physico-chimique, 75005 Paris, France.

low angle laser light scattering and gel permeation chromatography (9) (Table I). Osmolality of dextran solutions was adjusted with NaCl by using an Osmette Precision (freezing point) osmometer.

Washed RBCs were then suspended in PBS-dextran solution without glucose or human serum albumin and the cell volume fraction H was adjusted by usual microhematocrit technique. Heat treatment of RBCs between 46° and 49.5°C induces irreversible modification of the membrane protein spectrin without changing cell electrophoretic mobility (12) and intercell adhesiveness in PBS-dextran solution (12, 13). Nash and Meiselman (14) confirmed that dextran by itself has little effect on membrane elasticity and cell geometry. This heating technique thus provides a means to alter membrane mechanical properties and study the resultant alteration in the disaggregation behavior of cells. Glass tubes containing washed RBCs suspended in 2 g% DX 80-PBS at 45% hematocrit were heated at constant temperatures (48.4°, 48.8°, and 49.2°C) for 2 min before rapid cooling to room temperature. The temperature within the tube was controlled with Trendicator thermoelement (Omega Engineering, Inc., Stamford, CT).

Methods

Apparatus. The Couette flow system, shown in Fig. 1 *a*, consists of two transparent concentric cylinders (10-mm diam and 22-mm high for the inner cylinder) with an annular gap between them. The test sample of blood is placed in this gap of thickness $e = 0.5$ mm or $e = 1$ mm. The shear rate $\dot{\gamma} = V_0/e$ is generated across the gap by rotating the outer cylinder with a velocity V_0 through the servo-motor of a viscometer (Contraves LS 30, Zürich). The inner cylinder remains stationary, which prevents the formation of Taylor vortices. As the maximum Reynolds number $Re_{max} = \rho\,(V_0)_{max}e/\eta$ is lower than 60 (maximum velocity $[V_0]_{max} = 6.5$ cm/s, fluid viscosity $\eta > 10^{-2}$ dyn · s/cm^2, fluid density $\rho \simeq 1$ g/cm^3), laminar flow prevails. We further neglect the variations of the shear rate across the gap, and we assume a nearly uniform shear field in Couette flow. The plane Poiseuille flow was approximated by a flow channel of rectangular cross-section (width $h = 0.3$ mm and height $d = 15$ mm, Fig. 1 *b*). This channel was 20-cm long and opened at each end into a large tank. The volume flow rate Q was controlled with a calibrated peristaltic pump in the range 4×10^{-3}–1.5 cm^3/s (maximum Reynolds number $Re_{max} = \rho Q_{max}/[\eta d] \simeq 10^2$). The pulsatile part of the flow represents $< \pm 5\%$ of the volume flow rate Q with a frequency ranging between 2 and 2×10^2 Hz according to the speed of the electric driving motor. Continuous mechanical stirring in the tank feeding the Poiseuille flow avoids settling of cells before the blood entering the channel (15). The absence of significant spatial fluctuations along a vertical axis z* normal to the flow (see Fig. 1, *a* and *b*) in the steady-state reflectivity signal of the flowing suspension at low shear rates in Couette flow or low flow rates in plane Poiseuille flow gives experimental evidence of negligible sedimentation effects.

Multiple Light Scattering by Cell Suspensions. Multiple scattering of laser light by a collection of randomly separated and absorbing particles with sizes larger than the wavelength is essentially incoherent (no scattering interference between the wavelets scattered by the particles [19]). We may disregard the coherent backscattering occurring in a very sharp peak in the direction of the light source ($\theta = 0$, $\Delta\theta < \pi/360$) (37). Therefore, multiple scattering of light in erythrocyte suspensions may be modelled as consisting of photons of finite lifetime that diffuse through the medium (18, 19).[1] The backscattered intensity $I(\theta)$ at θ by a random collection of large particles involves the scattering angle θ, the scattering and absorption coefficients derived from the complex refractive indices of fluid and particles, the total scattering area σ of free surfaces of particles per volume of suspension (large particles scatter similarly to area-equivalent spheres [38, 39]), and the thickness of the scattering medium (18, 19). In the case of a collimated light source normal to a plane parallel slab containing the suspension, the scattering and absorption coefficients of the medium have no influence on the angular dependence of the backscattered flux[1] (Monte Carlo simulations give a nearly isotropic backscattering diagram $I[\theta] \simeq [\cos\theta]^{3/2}$ in agreement with experimental evidence[1]). We may thus define the relative scattered intensity $r(\theta) \simeq r(\cos\theta)^{3/2}$ referred to nonabsorbing particles (latex or glass spheres), where r is the diffuse reflectivity of the medium ($0 < r \leq 1$).

Cell aggregation reduces the total scattering area σ of free surfaces of cells per volume of blood and lowers the diffuse reflectivity r of the erythrocyte suspension (16). The reflectivity r for random cell orientation was related to the scattering area per volume of blood σ through the formula

$$\frac{\sigma}{\sigma_0} = \frac{r}{r_0}\left(\frac{1 - r_0}{1 - r}\right)^2 \simeq \frac{r}{r_0}, \tag{1}$$

where r_0 and σ_0 are the diffuse reflectivity and the scattering area per volume of blood in a reference state corresponding to complete dispersion and random orientation of the erythrocytes (16, 19).[1] Since $r_0 \simeq 0.15$ for an optically thick suspension of oxygenated cells (19) (washings in PBS ensure full oxygenation of cells) and $r \leq r_0$, we can approximate to good accuracy the ratio σ/σ_0 by r/r_0 (Eq. 1). The diffuse reflectivities r or r_0 depend on the thickness of the scattering medium and on cell oxygenation through the absorption coefficient, but the analysis of the reflectometric measurements relative to the reference state (r_0, σ_0) eliminates the influence of these parameters. Monte Carlo simulations for backscattering of light by blood support the above analytical expression (Eq. 1) (19).[1] We further define the reflectometric index $G = 1 - r/r_0 \simeq 1 - \sigma/\sigma_0 \simeq \sigma_A/\sigma_0$, where σ_A represents the total cell area participating in intercellular adhesion per volume of blood (σ_A counts the area from both adjacent cells as the light is not scattered by the bridging interface). The magnitude of the reflectometric index G thus provides a direct measure of the degree of cell aggregation.

The relationship $G = \sigma_A/\sigma_0$ is suitable for interpreting the macroscopic reflectivity measurements in Couette flow since the shear rate and the scattering area per volume of blood are nearly uniform across the gap. In a nonuniform-shear Poiseuille flow, the spatial variations of RBC aggregation across the channel lead to a complex reflectometric process. Taking a sufficiently small gap h between the plates ($h = 0.3$ mm) such that the transmittance across the channel is important, the photon density is approximately uniform within the suspension, and the backscattered flux exhibits nearly equal contributions from all the regions of the flow cross-section. Under such conditions ($h = 0.3$ mm, the characteristic penetration length of He-Ne laser light in blood at hematocrit 45% being ~0.5 mm [19][1]), we can approximately relate the macroscopic reflectometric index G to the bridging area per volume of blood $\langle\sigma_A\rangle$ averaged over the flow cross-section:

$$G = 1 - r/r_0 \simeq \frac{1}{h}\int_{-h/2}^{h/2}\frac{\sigma_A(y)}{\sigma_0}\,dy \simeq \frac{\langle\sigma_A\rangle}{\sigma_0}. \tag{2}$$

The above approximation becomes especially valid for near-complete cell dispersion through the flow cross-section ($\sigma_A(y) \simeq 0$, $-h/2 \leq y \leq h/2$).

TABLE I
ABSOLUTE AVERAGE MOLECULAR WEIGHTS OF DEXTRAN FRACTIONS

	Lot No.	M_w	M_n	M_z
DX 40	FL 18974	38,500	26,000	54,500
DX 80	HA 23155	72,500	47,000	109,000
DX 150	73F 03811	129,000	92,000	172,500
DX 500	GI 21917	415,000	187,000	961,000

Results from the authors (9).

[1]Mills, P., P. Snabre, and J. M. Aufrere, manuscript in preparation.

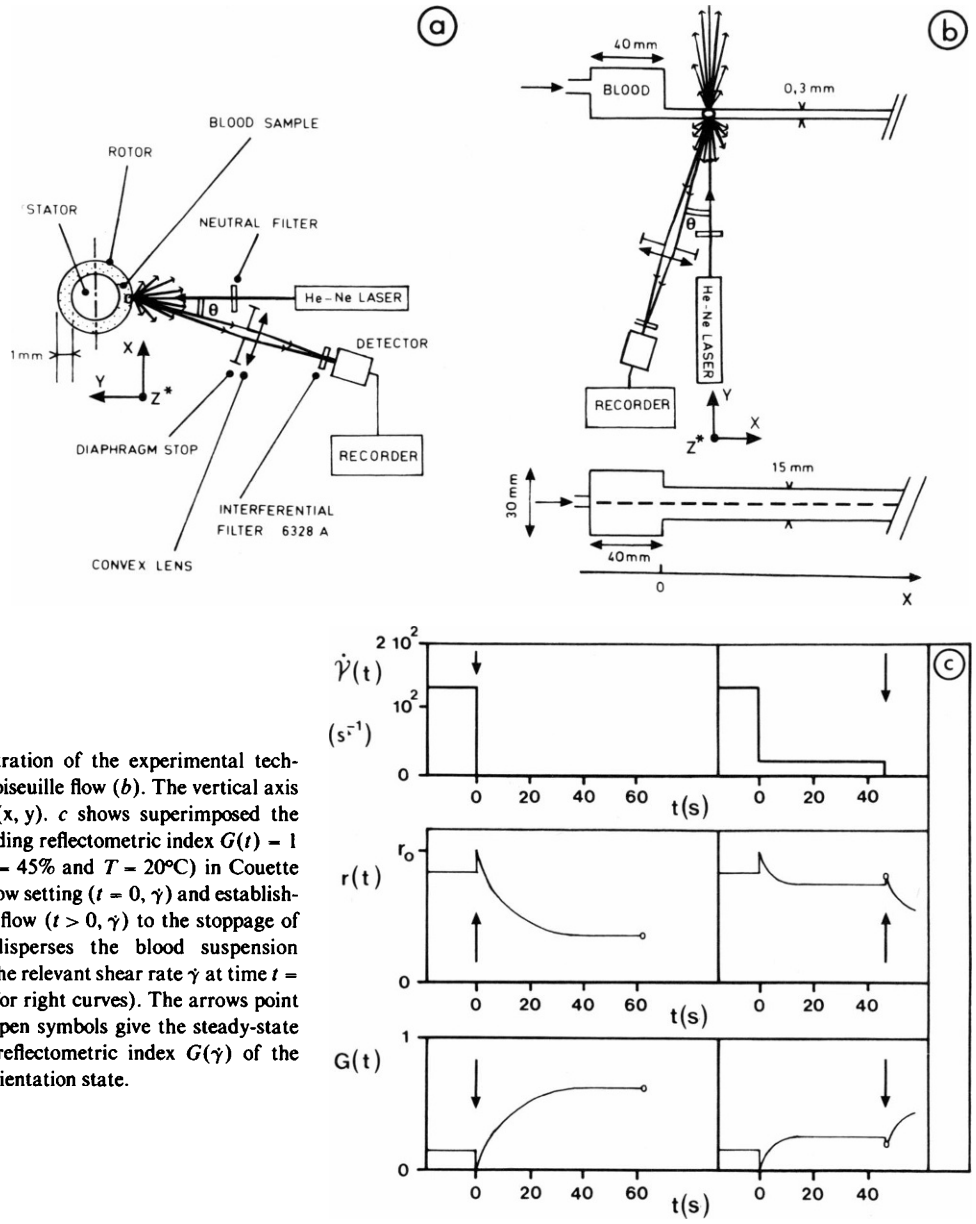

FIGURE 1 (*a* and *b*) Schematic illustration of the experimental techniques for Couette flow (*a*) and plane Poiseuille flow (*b*). The vertical axis z* is normal to the horizontal plane (x, y). *c* shows superimposed the reflectivity signal $r(t)$ and the corresponding reflectometric index $G(t) = 1 - r(t)/r_0$ for normal human blood ($H = 45\%$ and $T = 20°C$) in Couette geometry ($e = 1$ mm) from the time of flow setting ($t = 0, \dot{\gamma}$) and establishment of steady-state reflectance during flow ($t > 0, \dot{\gamma}$) to the stoppage of flow. An intense flow previously disperses the blood suspension ($t < 0, \dot{\gamma}_{max} = 128\ s^{-1}$) before imposing the relevant shear rate $\dot{\gamma}$ at time $t = 0$ ($\dot{\gamma} = 0$ for left curves and $\dot{\gamma} = 28\ s^{-1}$ for right curves). The arrows point out the time of flow stoppage and the open symbols give the steady-state reflectance $r(\dot{\gamma})$ and the steady-state reflectometric index $G(\dot{\gamma})$ of the flowing suspension for a random RBC orientation state.

The reflectometric technique thus provides a powerful way for determining the critical hydrodynamic conditions required for complete cell disaggregation in shear flow.

Reflectivity Measurements. Flow dependent changes of light reflection in concentrated RBC suspension subjected to shear flow were investigated at 20°C by illuminating the blood sample with a laser radiation (He-Ne laser; beam diameter 1 mm, wavelength $\lambda = 6328$ Å) perpendicular to the flow direction (16). The light flux backscattered by the flowing suspension was detected at small angles ($10° < \theta < 20°$) by a photometric device (Fig. 1, *a* and *b*). The radius of the transparent glass walls (~1 cm in Couette flow and infinite in plane Poiseuille flow), being much larger than the size of the scattering volume, we neglect the effect of wall curvature on reflectivity measurements.

Cell orientation occurs during flow for shear rates above $5\ s^{-1}$ and lowers the diffuse reflectivity of the suspension (16). Therefore, the flow was quickly stopped before any measurement (in 10^{-2} s) to suppress cell orientation. The analysis of the transient reflectivity signals $r(t)$ gives a time constant t_D for cell disorientation after flow stoppage of ~0.1s, showing no significant variation with the shear rate (16). Cell disorientation after flow stoppage results from the relaxation of cell deformation since the time course for the recovery of erythrocytes in a micropipette averages 0.15 s and shows no significant correlation with the degree of deformation (17) (microflows and cell re-aggregation also contribute in a less extent to the randomization of cell orientation). The reflectivity signal $r(t)$ thus reaches a peak value soon after flow stops because of the competition between the cell disorientation process (higher reflectivity) and the cell re-aggregation process (lower reflectivity). The time course t_D of the disorientation process ($t_D \simeq 0.1$ s), being much shorter than the time course t_A for cell re-aggregation ($5\ s < t_A < 100\ s$) for cells in PBS-dextran at hematocrit 45% [13]), the peak value of the reflectivity signal after flow stoppage characterizes the dynamical equilibrium aggregation for the flowing suspension in a random cell orientation state.

The reflectometric index $G = 1 - r/r_0$ of RBC suspensions was measured at various shear rates $\dot{\gamma}$ in Couette flow and at various volume flow rates Q in plane Poiseuille flow. The blood suspension was previously dispersed in an intense flow ($\dot{\gamma}_{max}$ or Q_{max}) before imposing the relevant flow ($\dot{\gamma}$ or Q) (Fig. 1 *c*). The reflectivity signal $r(t)$ decreases from the maximum value r_0 corresponding to the reference state of the suspension

just after the setting of flow ($\dot{\gamma}$ or Q) to reach a stationary level within 1 min. The peak value $r(\dot{\gamma})$ or $r(Q)$ of the reflectivity signal soon after flow stops characterizes the steady-state reflectance of the flowing suspension for a random orientation state of the erythrocytes. Fig. 1 *c* shows superimposed $r(t)$ and $G(t) = 1 - r(t)/r_0$ for human blood in Couette flow from the time of flow setting ($t = 0$) and establishment of steady-state aggregation during flow to the stoppage of flow. The time dependences of $r(t)$ in plane Poiseuille flow and Couette flow are qualitatively similar (15). Reflectivity measurements were performed at 10 cm downstream from the entrance of the rectangular channel. The establishment of steady-state aggregation in each volume of blood through the channel cross-section was verified by measuring the variations in the reflectance of the flowing suspension along the channel length from 1 mm to 10 cm downstream from the entrance. Steady-state conditions were always achieved for low dextran T500 concentrations in PBS ($\phi < 6$ g%). For higher dextran T500 concentrations ($\phi > 6$ g%), the steady-state reflectance was not established after passing the 10-cm point since the high viscosity of the suspending medium strongly increases the times of rouleaux formation (13) and delays the setting of steady-state aggregation in the channel (15).

Viscosity Measurements. The apparent relative viscosity η_r of red cell suspensions at various shear rates was measured at 20°C by using a Contraves LS 30 low shear viscometer. The blood sample was stirred before each measurement for avoiding sedimentation effects, and viscosities were calculated from the steady-state torque readings.

RESULTS

Cell Dispersion in Couette Flow

Influence of Hematocrit on Blood Dispersion in Couette Flow. Fig. 2 *a* displays the dependences of the reflectometric index $G(\dot{\gamma})$ upon the shear rate $\dot{\gamma}$ in normal red cells suspended at different hematocrit in PBS-1.2 g% dextran 80. The reflectometric index G decreases monotonically when the shear is raised above 1 s^{-1}, indicating a progressive shear-induced dispersion of cell rouleaux into smaller ones. Since complete dispersal of the cell suspension is only approached asymptotically (Fig. 2 *a*), we define the critical disaggregation shear rate $\dot{\gamma}_c$ by extrapolating to $G = 0$ the linear portion of the curves $G(\log \dot{\gamma})$ (Fig. 2 *a*). Raising the hematocrit shifts the critical shear rate $\dot{\gamma}_c$ towards lower values since the microrheological conditions around the cells and the relative viscosity $\eta_r(\dot{\gamma}, H)$ of the suspension strongly depend on the cell volume fraction (see Fig. 2 *b* and Table II). When plotting reflectometric data versus shear stress $\tau = \eta_S \eta_r(\dot{\gamma})\dot{\gamma}$ (η_S is the viscosity of the PBS-dextran solution), we obtain a single curve without significant dependence upon hematocrit (Fig. 3). The critical disaggregation shear stress τ_c defined in terms of extrapolated intercept thus directly reflects the mechanical force required to disrupt the bridging cells. Moreover, as shown in Table II, the product of the critical shear rate $\dot{\gamma}_c$ times the viscosity $\eta_S \eta_r(\dot{\gamma}_c, H)$ of the nearly dispersed suspension yields a good estimate of the critical shear stress τ_c ($\tau_c \simeq 2.5$ dyn/cm^2 for normal erythrocytes in PBS-1.2g% dextran T80, as shown in Fig. 3).

Influence of Cell Deformability on Blood Dispersion in Couette Flow. Let us now examine the influence of RBC deformability on cell dispersion in shear flow. Heat

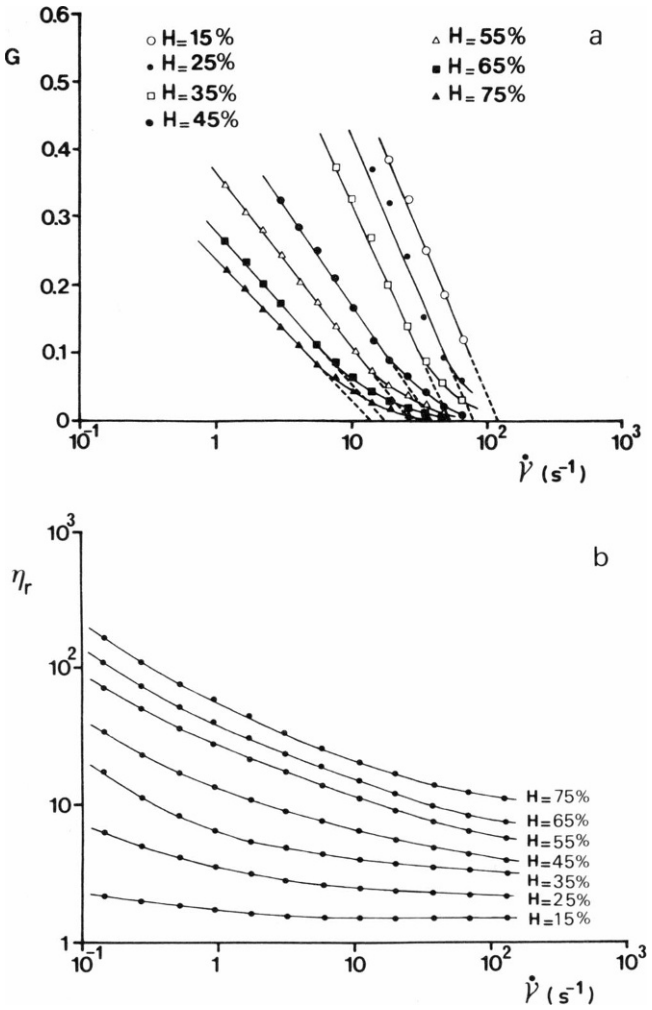

FIGURE 2 Plots of the reflectometric index G (*a*) and the relative viscosity η_r (*b*) against the shear rate $\dot{\gamma}$ in Couette flow for normal erythrocytes suspended at various hematocrit H in PBS-1.2 g% dextran T80 ($T = 20$°C and $\eta_S = 1.2$ centipoise). An extrapolation to the shear rates axis ($G = 0$) in *a* gives the critical shear rate $\dot{\gamma}_c$.

treatment of erythrocytes induces irreversible alterations in the endoface membrane proteins. The increase of rouleaux formation times at room temperature after RBC heat treatment reflects some loss in cell deformability (12, 13). The reflectometric index G of normal and heat-treated erythrocyte suspensions in PBS-2 g% dextran T80 ($H = 45\%$ and $T = 20$°C) is plotted as a function of shear rate in Fig. 4 *a*. Under defined shear rate conditions, the reduced membrane deformability of heat-treated red cells enhances the relative viscosity of the suspension (13) and improves the dissociation efficiency of the flow, resulting in shorter rouleaux and lower reflectometric index (Fig. 4 *a*). Heat treatment thus slightly lowers the critical disaggregation shear rate $\dot{\gamma}_c$ (Fig. 4 *a*). Plotting these reflectometric data versus the shear stress $\tau = \eta_S \eta_r(\dot{\gamma})\dot{\gamma}$, we get a single curve again, indicating that the critical disaggregation shear stress τ_c is without significant dependence on cell deformability (Fig. 4 *b*).

TABLE II
EXPERIMENTAL VALUES OF THE CRITICAL CONDITION PARAMETERS $\dot{\gamma}_c$ AND $\eta_S\eta_r(\dot{\gamma}_c, H)\dot{\gamma}_c$ IN COUETTE FLOW FOR NORMAL ERYTHROCYTES SUSPENDED AT DIFFERENT HEMATOCRIT IN PBS-1.2 g% DEXTRAN T80 (η_S = 1.2 CENTIPOISE)

H	$\dot{\gamma}_c(H)$	$\eta_r(\dot{\gamma}_c, H)$	$\eta_S\eta_r(\dot{\gamma}_c, H)\dot{\gamma}_c$
	s^{-1}		dyn/cm^2
0.15	120	1.51	2.19
0.25	79	2.25	2.14
0.35	53	3.47	2.2
0.45	38	4.89	2.23
0.55	25	7.95	2.38
0.65	17	12	2.45
0.75	13	18	2.81

Cell Dispersion in Shear Flow. The quantitation of shear forces for cell dispersion can provide a way for estimating the surface adhesive energy Γ in dynes per centimeter of the bridging membranes also called the fracture energy. We deliberately ignore the details of the physicochemical interactions generating the fracture energy (van der Waals and electrostatic interactions, polymer bridging, etc.). The dispersion of rouleaux by fluid stresses in a shear flow is a complex phenomenon that first requires that we examine the disruption process of two adhering erythrocytes. The adhesive energy of the contact area between cells is stored as a change in membrane strain energy (7, 25). The work done by mechanical shearing tends to overcome the adhesive energy of the doublet. Since a reduction in the bridging area of the doublet lowers the membrane strain energy, the external force required to laterally displace the axis of symmetry of cells gradually increases with the degree of cell separation. This behavior results from the ability of deformable particles to store elastic energy during aggregation and gradually restore this strain energy during separation (20, 21). The external

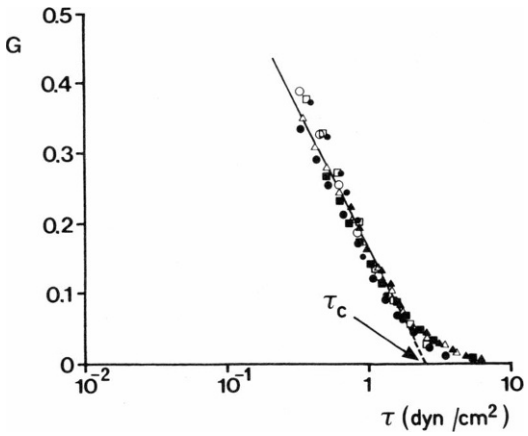

FIGURE 3 Relationship between reflectometric index G and shear stress τ in Couette flow for normal erythrocytes suspended at various hematocrit in PBS1.2 g% dextran T80. The symbols refer to the same hematocrit values as in Fig. 2. An extrapolation to the shear stresses axis (G = 0) gives the critical shear stress τ_c.

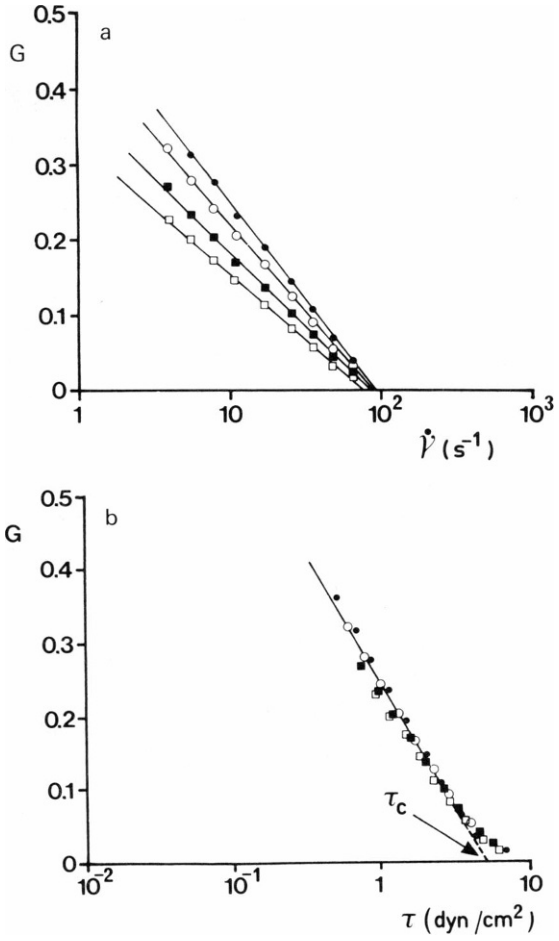

FIGURE 4 Plots of the reflectometric index G against the shear rate $\dot{\gamma}$ (a) or against the shear stress (b) in Couette flow for normal and heat-treated RBC in PBS-2 g% dextran T80 at 45% hematocrit (T = 20°C and η_S = 1.49 centipoise). An extrapolation to the shear stresses axis (G = 0) in b gives the critical shear stress τ_c. Normal RBC (●); T = 48.4°C (○); T = 48.8°C (■); T = 49.2°C (□).

shear force thus reaches a maximum value F_E near complete disruption of the doublet (21). The Derjaguin theory relates the disruption force F_E to the fracture energy Γ and to the mean curvature radius R_c of the bridging membranes just before the doublet rupture (21)

$$F_E = 2\pi R_c \Gamma. \quad (3)$$

Chien et al. (11) used a fluid mechanical method to measure the shear stress required to separate a two-cell rouleau in a flow channel under microscopic observation. The attachment of the doublet to the channel wall with the discoid faces of the cells parallel to the shearing stress prevents the two-cell rouleau from rotating. With increasing levels of shear stress, top and bottom cells are laterally separated in a gradual way by peeling, and the rupture of the doublet occurs for the critical shear stress τ_E(11). As the shearing stress acts over the upper area A_0 of the top cell, we can estimate the disruption force $F_E = \tau_E A_0$ from the critical shear stress τ_E and calculate the fracture energy Γ by using the Derjaguin relation (Eq. 3).

$$\Gamma = \frac{\tau_E A_0}{2\pi R_c}. \quad (4)$$

Using the flow channel technique, Jan (6) determined the shear stress τ'_E required to separate half of the doublet bridging interface for normal RBCs in PBS-dextran T80 (M_w 75,000). We made use of these data to get the disruption shear stress τ_E of a doublet incapable of rotating as a function of dextran T80 concentration (we take a ratio $\tau_E/\tau'_E = 2.4$ derived from the shear-stress dependence of the degree of doublet separation given in reference 11). The variations of the disruption shear stress τ_E versus dextran T80 concentration (Fig. 5) show a typical bell-shaped relationship (7). Erythrocyte disaggregation at high dextran concentrations likely results from an extension of the glycoproteic coat (22) and an enhancement of the repulsive electrostatic interactions (10; Snabre, P., and P. Mills, manuscript submitted for publication). Otherwise, we measured the critical shear stress τ_c in Couette flow for normal cells in PBS-dextran T80 (M_w 72,500) (Fig. 5). Under critical conditions ($\tau = \tau_c$), the mean bridging area per cell is only a few percent of total RBC area ($\sigma_A[\tau_c]/\sigma_0 \simeq 0.03$ as shown in Figs. 3 and 4 *b*). Therefore, we can reasonably consider this critical situation ($\tau = \tau_c$) as representative of near complete cell dispersal in shear flow and compare the critical shear stresses τ_c and τ_E. The experimental results displayed in Fig. 5 show that the critical shear stress τ_c in Couette flow exceeds by one order of magnitude the critical shear stress τ_E of a doublet incapable of rotating. Moreover, the ratio $\tau_c/\tau_E \simeq 10$ presents no remarkable change with dextran T80 concentration and consequently no significant dependence on intercell adhesiveness. The large difference between τ_c and τ_E was attributed by Chien et al. (11) to the difference in the directions in which the shearing forces act. Since the hydrodynamic force $F_c(\theta, \psi)$ acting on a nearly dispersed doublet in Couette flow ($\tau = \tau_c$) indeed changes with the doublet orientation in the shear field (23) (pushing the cells together when $-\pi/2 < \psi < 0$ and pulling them apart when $0 < \psi < \pi/2$), only a component of the overall shear stress τ_c induces cell disaggregation.

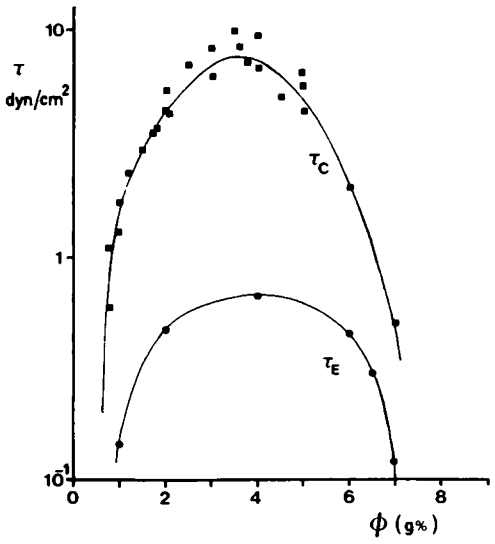

FIGURE 5 Critical shear stresses τ_c in Couette flow and τ_E in the flow channel experiment (Chien's technique [11]) plotted against the concentration ϕ of dextran T80 in PBS. The lower curve was obtained from Jan's data (6).

$$F_c(\theta, \psi) = \tau_c A_0 \sin(2\psi) \sin^2(\theta), \quad (5)$$

where θ and ψ are the spherical polar coordinates with respect to the vorticity axis of the shear flow. In a situation of near-complete cell dispersal ($\tau = \tau_c$), most triplets and higher rouleaux are immediately disrupted, and we can consider the flowing suspension as a dynamic system of transient doublets continuously colliding with the neighboring cells. The resulting set of transient doublets behave on a statistical basis as a suspension of rigid spheroids whose free rotation is prevented by particle crowding and presents an isotropic steady-state distribution of orientations (24). For critical conditions in shear flow, the doublets experience an average shearing force $\bar{F}_c = W\tau_c A_0$ equal to the disruption force F_E.

$$\bar{F}_c = W\tau_c A_0 = F_E = \tau A_0, \quad (6)$$

where W is a characteristic constant related to the random orientation of the transient doublets in critical shear flow. The comparison between the critical shear stresses τ_c and τ_E in Fig. 5 leads to $W \sim 0.1$. The critical shear stress τ_c derived from Eqs. 3 and 6 takes the form

$$\tau_c = \frac{2\pi R_c \Gamma}{W A_0}. \quad (7)$$

The above equation predicts no significant influence of cell volume fraction and membrane deformability on the critical shear stress τ_c for near-complete cell dispersion in agreement with the experimental results (Figs. 3 and 4 *b*).

This theoretical treatment thus provides a simple way for estimating the surface adhesive energy Γ of the bridging membranes from the experimental determination of the critical shear stress τ_c in Couette flow. For cells in 2 g% dextran T80 ($\tau_c \simeq 5$ dyn/cm^2 as shown in Fig. 4 *b*), we calculate from Eq. 7 a fracture energy $\Gamma \simeq 8.8\ 10^{-4}$ dyn/cm taking $R_c \simeq 10^{-4}$ cm, $A_0 \simeq 50\ 10^{-8}$ cm^2, and $W \simeq 0.1$. This estimate agrees fairly well with earlier computations of surface adhesive energy based on doublet shape and membrane properties (25), giving $\Gamma \simeq 10^{-3}$ dyn/cm for RBC aggregates formed by 2 g% of dextran with a molecular weight of 74,500 (this theoretical analysis uses the following experimental observation: the outer face of the end cell of a rouleau is concaved in 1 g% DX 80, becomes essentially flat in 2 g% DX 80, and is convexed in 4 g% DX 80 [25]).

Rouleaux Break-up in Shear Flow. The model presented in this section gives insight into the process of rouleaux disaggregation by fluid stresses in shear flow. The steady-state bridging area per volume of blood $\sigma_A(\tau)$ of the flowing RBC suspension results from the dynamical equilibrium process existing between aggregation and shear-induced dispersion of cells. Cell rouleaux can grow up until their size reaches a critical value above which the aggregates are immediately disrupted by shear forces. For any given shear stress τ, the mean size $R(\tau)$ of the aggregates then remains constant through addition and loss of cells. Let us consider N individual elastic particles of dimension a_0 forming a fractal aggregate of mean size R,

$$R \sim a_0 N^{1/D}, \tag{8}$$

where D is the fractal dimension introduced to describe the growth of particle clusters by aggregation (26). One of the authors (27) recently proposed a self-consistent field approximation to estimate the equilibrium size $R(\tau)$ of a fractal aggregate in a simple shear flow.

$$\frac{R(\tau)}{a_0} = 1 + \left[\frac{A\tau^*}{\tau}\right]^{1/(4-D)}, \tag{9}$$

where $\tau^* \sim \Gamma/a_0$ is a critical shear stress characterizing the intercell adhesiveness, and A is a constant. Moreover, this theoretical model gives an expression of the mean number $z(\tau)$ of contacts around every particle at a given shear stress τ.

$$z(\tau) = z_0\left[1 - \frac{a_0}{R(\tau)}\right] = \frac{z_0}{1 + \left(\frac{\tau}{A\tau^*}\right)^{1/(4-D)}}, \tag{10}$$

where z_0 is the maximum value of the mean coordination number $z(\tau)$. Since the mean coordination number z is directly proportional to the mean bridging area around every cell, the above equation (Eq. 10) yields the shear stress dependence of the equilibrium bridging area per volume of blood $\sigma_A(\tau)$.

$$\frac{\sigma_A(\tau)}{\sigma_M} = \frac{z(\tau)}{z_0} = \frac{1}{1 + \left[\frac{\tau}{A\tau^*}\right]^{1/(4-D)}}, \tag{11}$$

where σ_M is the maximum value of the equilibrium bridging area per volume of blood. Under low shear stress conditions, an aggregate consists of interconnected compact aggregates forming an irregular loose structure of fractal dimension $D \sim 2$ (26). When stresses tend to disperse the cells, the larger loose aggregates are separated into smaller compact ones (such as the rouleaux found in RBC suspensions) of fractual dimension $D \sim 3$. Therefore, we use Eq. 11 with the approximations $G = \sigma_A/\sigma_0$ and $D = 3$ for relating the macroscopic reflectometric index G to the shear stress and describing the disaggregation behavior of cell rouleaux in uniform-shear flow.

$$G(\tau) = \frac{\sigma_A}{\sigma_0} = \frac{\sigma_M/\sigma_0}{1 + \frac{\tau}{A\tau^*}}, \tag{12}$$

We investigated the reflectometric index G as a function of shear stress τ in Couette flow for normal erythrocytes in PBS-dextran solutions or human plasma (45% hematocrit, 20°C) (Fig. 6). For a given dextran concentration ϕ = 2 g%, the critical disaggregation shear stress τ_c defined as previously in terms of extrapolated intercept increases with the mass average molecular weight of the polymer indicating an increase in intercell adhesiveness (Fig. 6). Cells in human plasma (τ_c = 4.5 dyn/cm^2) display a disaggregation behavior nearly similar to cells in 2 g% dextran T80 ($\tau_c \simeq$ 5 dyn/cm^2). The maximum value σ_M of the bridging area per volume of blood was determined by measuring the equilibrium reflectometric index G_M of the suspension at low shear rates and by using the approximation $\sigma_M/\sigma_0 = G_M$. The parameter G_M characterizes the structure of the interconnected rouleaux network and keeps a nearly constant value G_M = 0.7 (Fig. 7, *inset*). A weak intercell adhesiveness yet prevents the stable formation of a gel-like structure and lowers the reflectometric index G_M at low shear rates (G_M = 0.3 for cells in 2 g% dextran T40). Substituting $A\tau^*$ by $\tau_c/10$ and σ_M/σ_0 by G_M into Eq. 12, the shear stress dependence of the reflectometric index $G(\tau)$ takes the form

$$G(\tau) = \frac{G_M}{1 + 10\tau/\tau_c}. \tag{13}$$

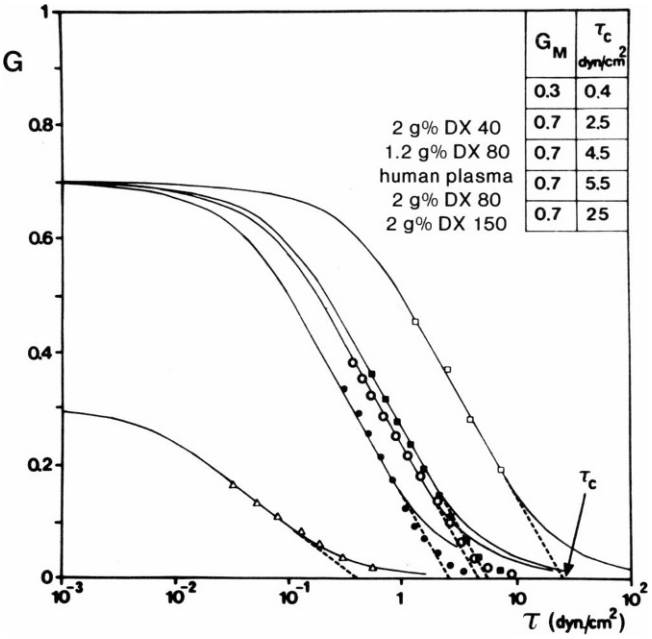

FIGURE 6 Relationship between reflectometric index G and shear stress τ in Couette flow for normal erythrocytes in PBS-dextran or human plasma at 45% hematocrit. 2 g% DX 40 (△), 1.2 g% DX 80 (●), human plasma (○), 2 g% DX 80 (■), 2 g% DX 150 (□). Solid curves are plots of Eq. 13 with the experimental values of G_M and τ_c shown in the inset.

Theoretical plots of the functions $G(\tau)$ (Eq. 13) using the experimental values of G_M and τ_c describe fairly well the reflectometric data (Fig. 6), although the curves $G_M(\tau)$ slightly deviate from the experimental points for shear stresses above τ_c (Fig. 6). The fracture energy is thus the only blood parameter influencing the critical shear stress $\tau_c = 10A\tau^* \sim \Gamma/a_0$ required for near-complete cell dispersal. Moreover, the correlation of the rouleaux break-up phenomenon with shear stress (Figs. 3 and 4 *b*) indicates that the parameter $z(\tau)/z_0$ (Eq. 11) in a concentrated suspension ($0.15 < H < 0.75$) is indeed essentially dependent on the shear stress and on the intercell adhesiveness, thus eliminating cell volume fraction and membrane deformability as possible factors.

Cell Dispersion in Plane Poiseuille Flow

Funadmental Analysis of Whole Blood Dispersion in Couette Flow and in Plane Poiseuille Flow. In this section, we propose a fundamental analysis of the contrast between cell disaggregation behavior in uniform Couette and nonuniform Poiseuille flows. For this purpose, we need to detail the calculation of the velocity profile of a non-Newtonian fluid in a plane Poiseuille flow. These theoretical considerations are limited to the case of cells in human plasma at 45% hematocrit since a general rheological law describing the shear-thinning behavior of concentrated cell suspensions is not yet available. The physical reason for the shear-thinning in blood suspension is mainly the dispersion of the aggregates (27, 34), but also the deformation and orientation of cells (28). For shear rates above 1 s^{-1}, Casson equation (Eq. 14) expresses fairly well the non-Newtonian features of whole blood (Fig. 7).

$$\tau^{1/2} = \tau_0^{1/2} + (\eta_\infty \dot{\gamma})^{1/2}, \tag{14}$$

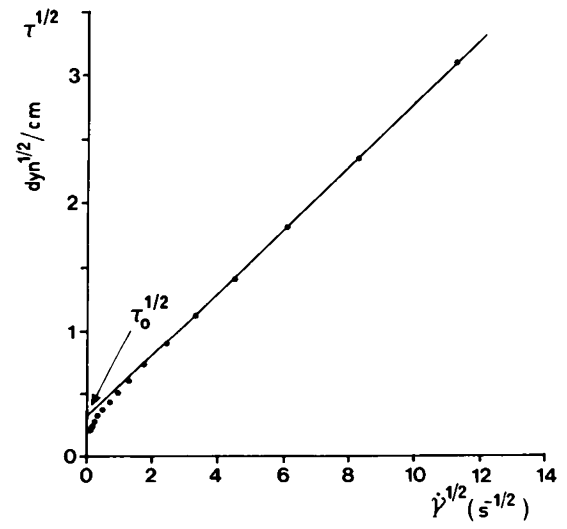

FIGURE 7 Casson's plot for normal human blood at 45% hematocrit and 20°C. An extrapolation to zero shear rate gives the yield stress $\tau_0 = 0.1$ dyn/cm^2. The viscosity parameter $\eta_\infty = 6$ centipoise is derived from the slope of the Casson plot for shear rates above 1 s^{-1}.

where τ_0 is the yield stress and η_∞ the viscosity of blood suspension at infinitely high shear rate. The yield stress τ_0 essentially involves the cell volume fraction H and the surface adhesive energy Γ (34). Viscosity measurements of normal cells at 45% hematocrit and 20°C temperature give $\tau_0 \simeq 0.1$ dyn/cm^2 and $\eta_\infty \simeq 6$ centipoise (Fig. 7). We define the pressure gradient $P < 0$ along the channel and we choose the y axis as normal to the flow such that the planes $y = 0$ and $y = h/2$ are assumed to mark the center plane and the inner wall of the channel (see Fig. 11 *b* in the Appendix with the condition $\delta = 0$ as the present section disregards the skimming layer effect). Substituting $\tau(y) = -Py$ into the Casson equation (Eq. 14), we obtain the shear rate $\dot{\gamma}(y)$ and the velocity profile $v(y)$ across the rectangular channel of thickness h and width $d(0 \le y \ll h/2)$. However, when y is such that $\tau_0 \ge -Py$, the velocity profile shows a central region of plug flow with strong RBC aggregation.

$$\begin{cases} \dot{\gamma}(y) = \dfrac{[\sqrt{-Py} - \sqrt{\tau_0}]^2}{\eta_\infty}, & -\tau_0/P \le y \le h/2 \\ \dot{\gamma}(y) = 0, & 0 \le y \le -\tau_0/P \end{cases} \tag{15}$$

$$v(y) = \int_y^{h/2} \dot{\gamma}(y)\, dy, \quad 0 \le y \le h/2. \tag{16}$$

The average velocity $\bar{V}$, the average shear rate $\langle\dot{\gamma}\rangle$, and the average shear stress $\langle\tau\rangle$ through the channel cross-section are expressed by:

$$\begin{cases} \bar{V} = \dfrac{2}{h}\displaystyle\int_0^{h/2} v(y)\, dy, \quad \langle\dot{\gamma}\rangle = \dfrac{2}{h}\int_0^{h/2} \dot{\gamma}(y)\, dy. \\ \langle\tau\rangle = \dfrac{2}{h}\displaystyle\int_0^{h/2} -Py\, dy = -\dfrac{Ph}{4} \end{cases} \tag{17}$$

From Eq. 12 and $\tau(y) = -Py$, we derive the bridging area per volume of blood $\langle\sigma_A\rangle$ averaged over the flow cross-section.

$$\frac{\langle\sigma_A\rangle}{\sigma_0} = \frac{2}{h}\int_0^{h/2} \frac{G_M}{(1 - 10\,Py/\tau_c)}\, dy, \tag{18}$$

with the substitutions $\sigma_M/\sigma_0 = G_M$ and $A\tau^* = \tau_c/10$ into Eq. 12.

A simple integration of the above equation together with the condition $\langle\tau\rangle = -Ph/4$ then gives the following analytical relation:

$$\frac{\langle\sigma_A\rangle}{\sigma_0} = \frac{G_M\tau_c}{20\langle\tau\rangle} \ln\left[1 + \frac{20\langle\tau\rangle}{\tau_c}\right]. \tag{19}$$

There is no need to know the shear rate profile $\dot{\gamma}(y)$ to derive the average shear stress dependence of $\langle\sigma_A\rangle/\sigma_0$ (Eq. 19) since $\sigma_A(y)$ is a function only of stress. The rheological parameters (η_∞, τ_0), however, influence the velocity profile $v(y)$, and the fluid rheology is needed to determine the average shear rate dependence of $\langle\sigma_A\rangle/\sigma_0$. We take $\tau_0 =$

0.1 dyn/cm^2, η_∞ = 6 centipoise, G_M = 0.7, and τ_c = 4.5 dyn/cm^2 (see Figs. 6 and 7) for applying these theoretical considerations to the case of whole blood with 45% hematocrit. The parameter $3\bar{V}/h = 3Q/h^2d$ yields a very good approximated value of the average shear rate $\langle\dot{\gamma}\rangle$ through the channel cross-section (see Fig. 12 of the Appendix). Therefore, we have plotted the reflectometric parameter $\langle\sigma_A\rangle/\sigma_0$ versus the macroscopic shear rate $\dot{\gamma}$ in Couette flow (Eqs. 13 and 14) or versus the variable $3\bar{V}/h \simeq \langle\dot{\gamma}\rangle$ in plane Poiseuille flow (Eqs. 14, 15, 17, and 19). It can be seen in Fig. 8 *a* that the curve for plane Poiseuille flow (full line *P*) deviates from the curve for Couette flow (full line *C*). The critical average disaggregation shear rate $3\bar{V}_c/h \simeq \langle\dot{\gamma}\rangle_c$ in Poiseuille flow defined in terms of extrapolated intercept exceeds by a factor of 2 the critical shear rate $\dot{\gamma}_c$ in Couette flow (Fig. 8 *a*).

Plotting the reflectometric parameter $\langle\sigma_A\rangle/\sigma_0$ versus the average shear stress $\langle\tau\rangle$ gave similar results (full lines in Fig. 8 *b* using Eqs. 13 and 19) with a ratio $\langle\tau\rangle_c/\tau_c$ of the critical shear stresses $\langle\tau\rangle_c$ in plane Poiseuille flow and τ_c in Couette flow close to 2 (Eqs. 13 and 19 further predict no variation of this ratio with intercell adhesiveness). This difference results from the non-uniform shear field in Poiseuille flow. Indeed, the flow in the core region is not sufficiently intense to disperse RBC rouleaux as much as in the other regions of the channel where the flow intensity is greater. A higher average shear stress $\langle\tau\rangle_c \simeq 2\ \tau_c$ is thus required in plane Poiseuille flow especially to disperse the rouleaux flowing near the centerplane $y = 0$ of the rectangular channel. The flow geometry thus influences the critical conditions parameters $\langle\dot{\gamma}\rangle_c$ and $\langle\tau\rangle_c$ representative of near-complete cell dispersal over the whole flow cross-section.

Let us now consider the effect of plasma skimming on the velocity profile and on cell disaggregation behavior in Couette flow and plane Poiseuille flow. Erythrocyte aggregation favors the formation of a plasma layer near the vessel walls (30, 36). This layer is responsible for the Fahraeus and Fahraeus Lindqvist effects in the vessels (29). A simple hydrodynamic calculation gives the average velocity $\bar{V}$, the average shear stress $\langle\tau\rangle$, and the average bridging area per volume of blood $\langle\sigma_A\rangle$ in the presence of a plasma layer of thickness δ (see Appendix). The existence of a plasma layer in Couette flow (δ = 20 μm and e= 1 mm) slightly alters the bridging area per volume of blood–shear rate relationship without changing the critical disaggregation shear rate $\dot{\gamma}_c$ (Fig. 8 *a*, dashed line C). Considering a plasma layer thickness δ = 20 μm and a channel gap h = 0.3 mm, the approximation $3\bar{V}/h = \langle\dot{\gamma}\rangle$ still applies with a good accuracy for average shear rates $\langle\dot{\gamma}\rangle$ over the flow cross-section above 1 s^{-1}, as shown in the Appendix (Fig. 12). Plasma skimming in plane Poiseuille flow leads to an important reduction in the effective average shear rate experienced by cells and thus enhances the critical average disaggregation shear rate $3\bar{V}_c/h \simeq \langle\dot{\gamma}\rangle_c$ (8 *a*, dashed line P). Yet, the average bridging area per volume of blood–average shear stress relationship remains nearly unchanged in the presence of a plasma layer (dotted lines C for Couette flow and P for plane Poiseuille flow in Fig. 8 *b*) since the local bridging area per volume of blood $\sigma_A(y)$ is a function only of the local shear stress $\tau(y) = -Py$ (Eq. 12). The critical disaggregation shear

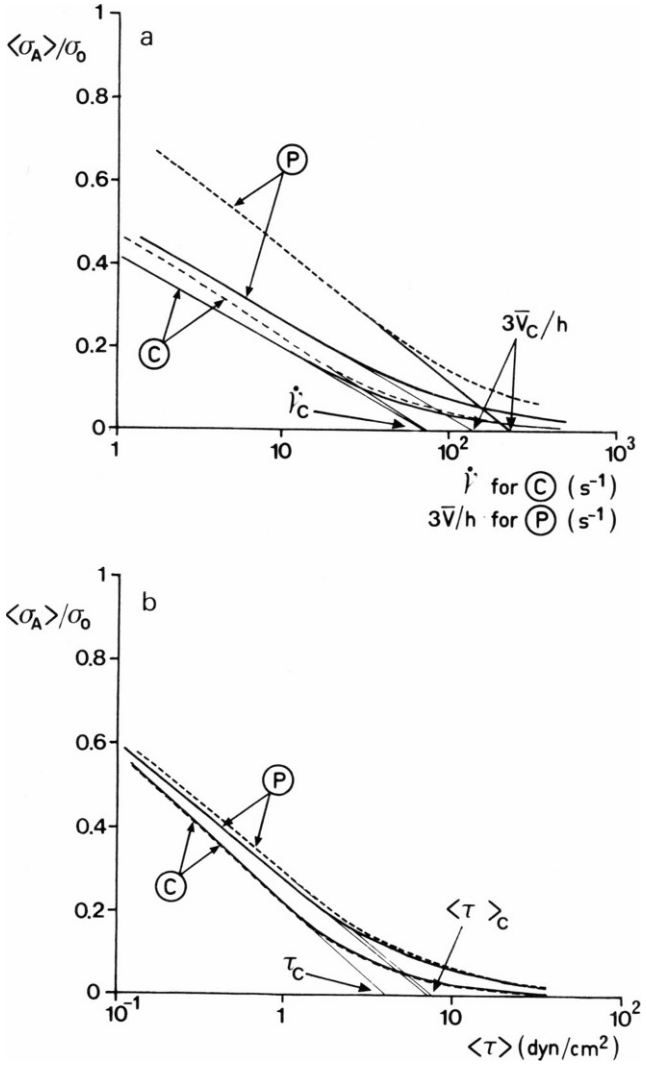

FIGURE 8 (*a*) Theoretical plots of $\langle\sigma_A\rangle/\sigma_0$ for human blood against the shear rate $\dot{\gamma}$ in Couette flow (*C*) or against the parameter $3\bar{V}/h$ in plane Poiseuille flow (*P*). (*b*) Theoretical plots of $\langle\sigma_A\rangle/\sigma_0$ for human blood against the average shear stress $\langle\tau\rangle$ in Couette flow (*C*) and plane Poiseuille flow (*P*). Solid lines indicate an absence of plasma skimming (δ = 0), whereas dashed lines are relative to a plasma layer thickness δ = 20 μm. We take τ_0 = 0.1 dyn/cm^2, τ_c = 4.5 dyn/cm^2, η_S = 1.6 centipoise, η_∞ = 6 centipoise, and G_M = 0.7 for human blood at 45% hematocrit and 20°C temperature. The average shear stress dependence of $\langle\sigma_A\rangle/\sigma_0$ without plasma skimming (δ = 0) is calculated from Eq. 12 in Couette flow and from Eq. 19 in plane Poiseuille flow. Eqs. A3 and A4 in the Appendix give the average velocity $\bar{V}(\tau_0, \eta_S, \eta_\infty, P, h, \delta)$ and the average shear stress $\langle\tau\rangle = -Ph/4$ through the rectangular channel in the presence of a plasma layer with thickness δ. The average shear rate and average shear stress dependences of the reflectometric parameter $\langle\sigma_A\rangle/\sigma_0$ are then derived from Eq. A2 in Couette flow (e = 1 mm) and from Eq. A5 in plane Poiseuille flow (h = 0.3 mm).

stresses τ_c in Couette flow and $\langle\tau\rangle_c \simeq 2\ \tau_c$ in plane Poiseuille flow only reflect the intercell adhesiveness, thus eliminating the plasma layer thickness as a possible factor.

Experimental Cell Disaggregation Behavior in Couette Flow and Plane Poiseuille Flow. In the present section, we investigate the disaggregation behavior of cell suspensions by the light reflectometry technique in Couette flow ($e = 1$ mm) and in plane Poiseuille flow ($h = 0.3$ mm). We performed the reflectivity measurements in the rectangular channel by imposing the volume flow rate Q. In Fig. 9, we have plotted the measured reflectometric index G versus the macroscopic shear rate in Couette flow or versus the parameter $3\bar{V}/h = 3Q/h^2d$ in plane Poiseuille flow for normal erythrocytes in PBS-dextran T500 at 45% hematocrit. Since the flow parameter $3\bar{V}/h$ approximates fairly well the average shear rate $\langle\dot{\gamma}\rangle$ through the channel cross-section, these experimental data indicate a significant difference between the reflectometric curves $G(3\bar{V}/h) \simeq G(\langle\dot{\gamma}\rangle)$ for plane Poiseuille flow and the corresponding curves $G(\dot{\gamma})$ for Couette flow (Fig. 9). As previously, we define the critical condition parameter $3\bar{V}_c/h$ for near-complete cell dispersal in plane Poiseuille flow as the intersection on the shear rate axis ($G = 0$) with a straight line fitting the middle part of the reflectometric curve $G(3\bar{V}/h)$. The critical average shear rate $3\bar{V}_c/h \simeq \langle\dot{\gamma}\rangle_c$ in plane Poiseuille flow exceeds by a factor of 3 to 4 the critical shear rate $\dot{\gamma}_c$ in Couette flow (Fig. 10). The ratio of the critical condition parameters $3\bar{V}_c/h$ and $\dot{\gamma}_c$, remaining almost constant over a wide dextran T500 concentration range (Fig. 10), is thus nearly independent of intercell adhesiveness. Considering both the effect of the velocity profile and that of a plasma layer of thickness $\delta = 20\ \mu$m, the fundamental analysis developed in the last section predicts a theoretical ratio $\langle\dot{\gamma}\rangle_c/\dot{\gamma}_c = 3.3$ for whole blood (Fig. 8 *a*, *dashed curves*) in good agreement with experimental results. Complete cell dispersal through the entire flow cross-section thus requires a higher average shear rate $\langle\dot{\gamma}\rangle_c$ in plane Poiseuille flow than in Couette flow because of the nonuniform shear field in the channel and the formation of a plasma layer.

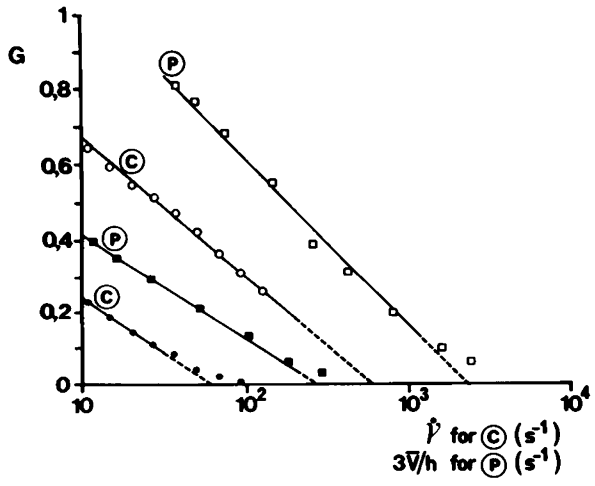

FIGURE 9 Plots of the reflectometric index G against the shear rate $\dot{\gamma}$ in Couette flow (C) or against the parameter $3\bar{V}/h$ in plane Poiseuille flow (P) for normal erythrocytes suspended at 45% hematocrit in PBS-0.5 g% dextran T500 (● and ■), and PBS-3.5 g% dextran T500 (○ and □).

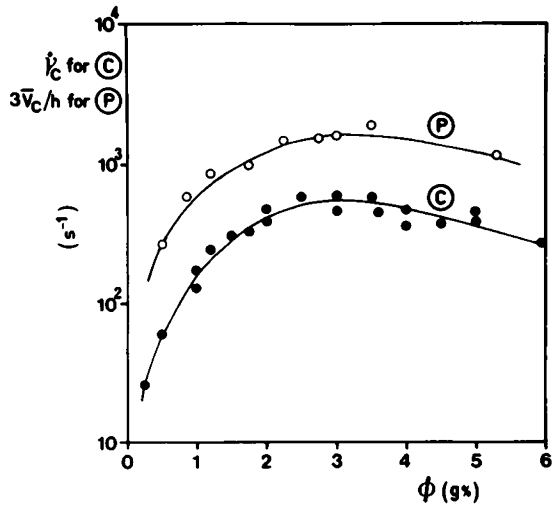

FIGURE 10 Critical shear rate $\dot{\gamma}_c$ in Couette flow (C) and critical condition parameter $3\bar{V}_c/h$ in plane Poiseuille flow (P) plotted against the concentration ϕ of dextran T500 in PBS (45% hematocrit).

Role of Erythrocyte Aggregation in the Microcirculation. This study raises important questions concerning the role of RBC aggregation in the microcirculation. It is possible from the present analysis to draw out some conclusions about blood circulation in large vessels several centimeters long (the last condition ensures the establishment of steady-state aggregation across the flow cross-section of the vessel). Since the pressure gradient P characterizes the different parts of the microcirculation, the reliable flow parameter in vessels is the cross-sectional average shear stress $\langle\tau\rangle$. The intercell adhesiveness is the only parameter influencing the critical average shear stress for near-complete cell dispersal, thus eliminating cell volume fraction, membrane properties, and plasma skimming as possible factors. For normal whole blood, the critical average shear stress $\langle\tau\rangle_c \simeq 9$ dyn/cm^2 in plane Poiseuille flow exceeds by a factor of 2 the critical disaggregation shear stress $\tau_c \simeq 4.5$ dyn/cm^2 in Couette flow. The critical wall shear stress τ_w for near-complete cell dispersion of normal whole blood in a large vessel is thus close to 18 dyn/cm^2 ($\tau_w = 2\langle\tau\rangle_c$). The last value is not far from the physiological values of the wall shear stress in the venous microcirculation (31), representing ~70% of the vascular bed volume. Under physiological conditions, the wall shear stress in small veins (0.11–0.5-mm diam, 5–10-mm long, 10–25% of the vascular bed volume [31, 36]) and main venous branches (0.1–2.3-mm diam, 20–100-mm long, 20–30% of the vascular bed volume [31, 35]) ranges from

10 to 60 dyn/cm^2 (31). Therefore, the present study predicts that cell aggregation slightly persists near the centerline of some large veins in the normal microcirculation. Intravascular red cell aggregation was indeed observed in some parts of the venous microcirculation (32). An increase in cell surface adhesive energy (observed in some pathological cases such as leukemia or diabetes [33]) results in a higher critical wall shear stress τ_w and enhances the intravascular erythrocyte aggregation.

CONCLUSION

An important result arises from the present work: the plot of the equilibrium reflectometric index $G \simeq \sigma_A/\sigma_0$ of the blood suspension against the shear stress τ experienced by cells in a uniform-shear flow provides a powerful means for studying the main features of the cell disaggregation process and for determining the erythrocyte surface adhesive energy Γ. This investigation indeed shows that the intercell adhesiveness is the only blood parameter influencing rouleau break-up in Couette flow, thus eliminating hematocrit and cell membrane deformability as possible factors. Among other advantages, this allows one to compare the critical condition parameters representative of near-complete cell dispersion in different hydrodynamic situations, irrespective of the hematocrit conditions. The disruption shear stress τ_E of an isolated doublet incapable of rotating (flow channel technique) indeed exceeds by one order of magnitude the critical disaggregation shear stress τ_c in Couette flow, independently of intercell adhesiveness. This behavior likely results from the isotropic steady-state distribution of orientations for the transient doublets near complete cell dispersal in Couette flow. Otherwise, complete cell disaggregation in plane Poiseuille flow requires a higher average shear rate $3\bar{V}_c/h \simeq \langle\dot{\gamma}\rangle_c$ than in uniform-shear Couette flow, arising from the flattening of the velocity profile in the central region of the channel and from the formation of a plasma layer. The ratio of the critical conditions parameters $3\bar{V}_c/h$ for plane Poiseuille and $\dot{\gamma}_c$ for Couette flow presents no significant variation with intercell adhesiveness ($3 < 3\bar{V}_c/h\dot{\gamma}_c < 4$). A fundamental analysis of rouleaux break-up in shear flow further predicts that the average critical shear stress $\langle\tau\rangle_c$ for near-complete cell dispersion in plane Poiseuille flow is about twice the critical shear stress τ_c in Couette flow, irrespective of intercell adhesiveness. Finally, the present work provides a way for quantitatively estimating the surface adhesive energy Γ of cell aggregates by fluid mechanical technique.

APPENDIX

We consider a division of blood flow into two regions: the plasma layer near the walls (of Newtonian viscosity η_S and thickness δ) and the blood suspension in the core of the flow (of non-Newtonian viscosity η obeying Casson Eq. 14) (Fig. 11). We choose the y axis as normal to the flow, and we neglect the variation in the hematocrit in the presence of a plasma layer.

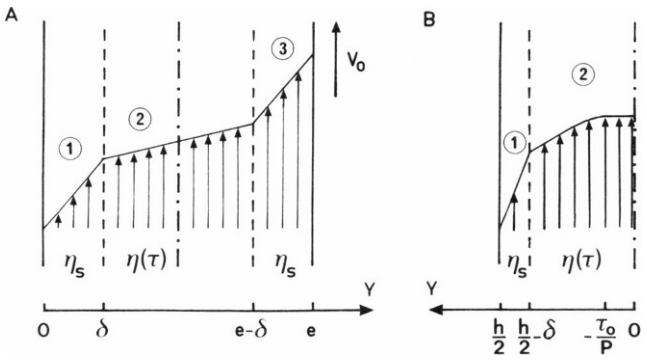

FIGURE 11 Schematic representation of the biphasic flow of blood in Couette geometry (*A*) and in plane Poiseuille geometry (*B*). Regions 1 or 3 are associated with the plasma layer (thickness δ, viscosity η_S), and region 2 corresponds to the blood suspension in the core of the flow. The horizontal axis y is normal to the flow.

Couette Flow

The macroscopic shear rate $\dot{\gamma}$ is defined as V_0/e, where V_0 is the velocity of the outer cylinder and e is the gap thickness (Fig. 11 *a*). The continuity of fluid velocity and shear stress at the boundaries $y = \delta$ and $y = e - \delta$ between plasma layer (regions 1 and 3 in Fig. 11 *a*) and blood suspension (region 2 in Fig. 11 *a*) together with the Casson equation (Eq. 14) allow the calculation of the uniform-shear rate $\dot{\gamma}_2(y)$ experienced by cells in the core of the flow (region 2). Furthermore, the Casson model gives no shear in the core for shear stresses $\tau(\dot{\gamma})$ lower than the yield-stress τ_0.

$$\begin{cases} \dot{\gamma}_2(y) = \dfrac{\dot{\gamma}}{1 + \dfrac{2\delta}{e}\left(\dfrac{\eta(\dot{\gamma}_2)}{\eta_S} - 1\right)}, \\ \tau(\dot{\gamma}) = \eta(\dot{\gamma}_2)\dot{\gamma}_2 > \tau_0 \\ \dot{\gamma}_2(y) = 0, \quad \tau(\dot{\gamma}) < \tau_0 \end{cases}$$

$$\text{with } \eta(\dot{\gamma}_2) = [(\tau_0/\dot{\gamma}_2)^{1/2} + \eta_\infty^{1/2}]^2. \tag{A1}$$

From Eq. 12 giving $\sigma_A(\tau)$, we then deduce the expression $\sigma_A(\dot{\gamma})$ for the bridging area per volume of blood in the presence of a plasma layer:

$$\frac{\sigma_A}{\sigma_0} = \frac{\sigma_M/\sigma_0}{1 + \tau/A\tau^*} \text{ with } \tau(\dot{\gamma}) = \eta(\dot{\gamma}_2)\dot{\gamma}_2. \tag{A2}$$

Plane Poiseuille Flow

The condition $\tau = -Py$, together with the Casson equation (Eq. 14), allows the calculation of the shear rate $\dot{\gamma}_1(y)$ in the plasma layer (region 1 in Fig 11 *b*) and $\dot{\gamma}_2(y)$ in the core of the suspension (region 2 in Fig. 11 *b*).

$$\left.\begin{aligned} \dot{\gamma}_1(y) &= \frac{Py}{\eta_S}, && \frac{h}{2} - \delta \le y \le \frac{h}{2} \\ \dot{\gamma}_2(y) &= [\sqrt{-Py} - \sqrt{\tau_0}]^2\eta_\infty^{-1}, && -\tau_0/P \le y \le \frac{h}{2} - \delta \\ \dot{\gamma}_1(y) &= 0, && 0 \le y \le -\tau_0/P \end{aligned}\right\}, \tag{A3}$$

where $P < 0$ is the pressure gradient along the channel. The average velocity $\bar{V}$, average shear rate $\langle\dot{\gamma}\rangle$, and average shear stress $\langle\tau\rangle$ through the channel cross-section then obey:

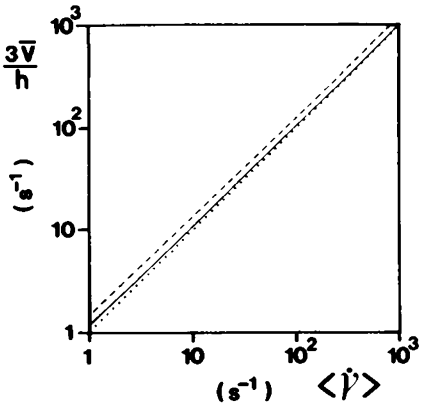

FIGURE 12 Theoretical plots of the flow parameter $3\bar{V}/h$ versus the average shear rate $\langle\dot{\gamma}\rangle$ in plane Poiseuille flow for normal human blood. The solid line for $\delta = 0$ and the dashed line for $\delta = 20$ μm are derived from Eqs. A3 and A4 in the Appendix taking $\tau_c = 4.5$ dyn/cm², $\tau_0 = 0.1$ dyn/cm², $h = 0.3$ mm, $\eta_S = 1.6$ centipoise, and $\eta_\infty = 6$ centipoise. The dotted line shows the approximation $\langle\dot{\gamma}\rangle = 3\bar{V}/h$.

$$\left.\begin{aligned} \bar{V} &= \frac{2}{h}\int_0^{h/2}\left[\int_y^{h/2}\dot{\gamma}(y)\,dy\right]dy \\ \langle\dot{\gamma}\rangle &= \frac{2}{h}\int_0^{h/2}\dot{\gamma}(y)\,dy \\ \text{and}\quad \langle\tau\rangle &= \frac{2}{h}\int_0^{h/2} -Py\,dy = -\frac{Ph}{4} \end{aligned}\right\}. \qquad \text{(A4)}$$

From Eq. 12, we then deduce the bridging area per volume of blood $\langle\sigma_A\rangle$ averaged over the core flow section ($0 \le y \le h/2 - \delta$)

$$\frac{\langle\sigma_A\rangle}{\sigma_0} = \frac{1}{\left(\frac{h}{2}-\delta\right)}\int_0^{h/2-\delta}\frac{\sigma_M/\sigma_0}{(1+\tau/A\tau^*)}\,dy, \qquad \text{(A5)}$$

with $\tau = -Py$.

For a non-Newtonian whole blood at 45% hematocrit and without plasma layer ($\delta = 0$), the flow parameter $3\bar{V}/h$ approximates with a very good accuracy the average shear rate $\langle\dot{\gamma}\rangle$ (full line in Fig. 12). This approximation still applies reasonably in the presence of a plasma layer (dotted line in Fig. 12 with $\delta = 20$ μm and $h = 300$ μm).

We gratefully acknowledge the referees for their very useful comments and their efforts to achieve greater clarity in the expression of this topic.

Received for publication 25 July 1985 and in final form 17 November 1986.

REFERENCES

1. Chien, S. 1972. Present state of blood rheology. In hemodilution. Theoretical basis and clinical application. *Int. Symp. Rottach.* Egern 1971, Karger, Basel. 1–45.
2. Fahraeus, R. 1929. The suspension stability of the blood. *Physiol. Rev.* 9:241.
3. Chien, S., S. Usami, H. M. Taylor, J. L. Lunberg, and M. I. Gregersen. 1966. Effect of hematocrit and plasma proteins on human blood rheology at low shear rates. *J. Appl. Physiol.* 21:81–87.
4. Brooks, D. E. 1973. The effect of neutral polymer on the electrokinetic potential of cells and other charged particles. IV Electrostatic effects in dextran mediated cellular interactions. *J. Colloid Interface Sci.* 43:714–726.
5. Chien, S., and K. M. Jan. 1975. Red cell aggregation by macromolecules: roles of surface adsorption and electrostatic repulsion. *J. Supramol. Struct.* 1:385–395.
6. Jan, K. M. 1979. Red cell interactions in macromolecular suspension. *Biorheology.* 16:137–148.
7. Chien, S., L. A. Sung, S. Simchon, M. L. Lee, K. M. Jan, and R. Skalak. 1983. Energy balance in red cell interactions. *Ann. NY Acad. Sci.* 416:190–206.
8. Evans, E., and B. Kukan. 1983. Free energy potential of erythrocytes and phosphatidylcholine/phosphatidylserine vesicles in dextran (36 500 MW) solutions and in plasma. *Biophys. J.* 44:255–260.
9. Snabre, P., G. Grossman, and P. Mills. 1985. Effect of dextran polydispersity on red blood cell aggregation. *Colloid & Polymer. Sci.* 263:478–483.
10. Snabre, P., and P. Mills. 1986. Role des interactions électrostatiques dans les phénomènes d'agrégation érythrocytaire. Hémorhéologie et agrégation érythrocytaire. Ed. Medicales Internationales, Groupe Lavoisier. 98–110.
11. Chien, S., G. L. A. Sun, S. Kim, A. M. Burke, and S. Usami. 1977. Determination of aggregation force in rouleaux by fluid mechanical technique. *Microvasc. Res.* 13:327–333.
12. Rakow, A., S. Simchon, L. A. Sung, and S. Chien. 1981. Aggregation of red cells with membrane altered by heat treatment. *Biorheology.* 18:3–8.
13. Snabre, P., H. Baumler, and P. Mills. 1985. Aggregation of human red blood cells after moderate heat treatment. *Biorheology.* 22:185–195.
14. Nash, G. B., and H. J. Meiselman. 1983. Effects of dextran and polyvinylpyrrolidone on red cell geometry and membrane elasticity. *Ann. NY Acad. Sci.* 416:255–262.
15. Bitbol, M. 1983. Effects d'entrée dans un conduit de dimension artériolaire. *Innov. Tech. Biol. Med.* 4(special issue):336–341.
16. Mills, P., D. Quemada, and J. Dufaux. 1980. Etude de la cinétique d'aggrégation érythrocytaire dans un écoulement de Couette. *Rev. Phys. Appl.* 15:1357–1366.
17. S. Chien, K. L. P. Sung, R. Skalak, S. Usami, and A. Tözeren. 1978. Theoretical and experimental studies on viscoelastic properties of erythrocyte membrane. *Biophys. J.* 24:463–487.
18. Mills, P., and J. M. Aufrere. 1983. Diffusion multiple d'un faisceau lumineux par une suspension de particules. Techniques avancées en hémorhéologie. DPIC-INPL Ed., Nancy, France. 543–579.
19. Mills, P., and P. Snabre. 1983. Agregometrie optique de la suspension sanguine. Techniques avancées en hémorhéologie. DPIC-INPL Ed, Nancy, France. 580–598.
20. Johnson, K. L., K. Kendall, and A. D. Roberts. 1971. Surface energy and the contact of elastic solids. *Proc. Roy. Soc. A.* 324:301–313.
21. Derjaguin, B. V., V. M. Muller, and Yu. P. Toporov. 1975. Effect of contact deformations on the adhesion of particles. *J. Colloid Interface Sci.* 53:314–326.
22. Snabre, P., and P. Mills. 1985. Effect of dextran polymer on glycocalyx structure and cell electrophoretic mobility. *Colloid & Polym. Sci.* 263:494–500.
23. Goldsmith, H. L., O. Lichtarge, M. Tessier-Lavigne, and S. Spain. 1981. Some model experiments in hemodynamics. VII. Two body collisions between blood cells. *Biorheology.* 18:531–555.
24. Anczwrowski, E., and S. G. Mason. 1967. The kinetics of flowing dispersions. III. Equilibrium orientations of rods and discs. *J. Colloid Interface Sci.* 23:533–546.
25. Skalak, R., P. R. Zarda, K. M. Jan, and S. Chien. 1981. Mechanics of rouleau formation. *Biophys. J.* 35:771–781.
26. Kolb, M., and R. Jullien. 1984. Chemically limited versus diffusion limited aggregation. *J. Phys. Lett.* 45:L.977–L.981.
27. Mills, P. 1985. Non-Newtonian behavior of floculated suspensions. *J. Phys. Lett.* 46:L301–L309.
28. Merrill, E. W., and G. A. Pelletier. 1967. Viscosity of human blood:

transition from Newtonian to non-Newtonian. *J. Appl. Physiol.* 23:178–182.

29. Gaehtgens, P., F. Kreutz, and K. H. Albrecht. 1978. Fahraeus effect and cell screening during tube flow of human blood. II. Effect of dextran-induced cell aggregation. *Biorheology.* 15:155–161.
30. Yardin, G., and J. Dufaux. 1983. Visualisation, par microscope, d'écoulements de suspensions de globules rouges dans des capillaires cylindriques. Essai de modélisation. *Innov. Tech. Biol. Med.* 4(special issue): 119–126.
31. Sutera, S. P. 1977. Red cell motion and deformation in the microcirculation. *Cardiovasc. Pulmonary Dynamics.* 71:211–242.
32. Vejlens, G. 1962. Theses and hypotheses concerning intravasal erythrocyte aggregation. *Biorheology.* 1:71–72.
33. Othmane, A., M. Bitbol, C. Bucherer, P. Mills, P. Snabre, C. Lacombe, and J. C. Lelievre. 1985. Comparison between light reflectometry and viscometry for RBC aggregation assessment in diabetes. *Clin. Hemorheology.* 5:561–572.
34. Mills, P., and P. Snabre. 1987. The fractal concept in the rheology of concentrated suspensions. *Rheol. Acta.* In press.
35. Hamilton, W. F., and P. Dow, editors. 1963. Handbook of Physiology. Section 2. Circulation, Vol. II. American Physiological Society.
36. Mills, P., and P. Snabre. 1987. Particle migration connected to rheological mechanisms in a flowing aggregated suspension. Application to white blood cells migration. *Biorheology.* In press.
37. Wolf, P. E., and G. Maret. 1985. Weak localization and coherent back-scattering of photons in disordered media. *Phys. Rev. Lett.* 55:2696–2699.
38. Van De Hulst, H. C. 1980. Multiple Light Scattering. Vols. 1 and 2. Academic Press, Inc., New York.
39. Glantschnig, W. J., and S. H. Chen. 1981. Light scattering from water droplets in the geometrical optics approximation. *Appl. Opt.* 20:2499–2509.